EAI Endorsed Transactions
on Energy Web
Research Article EAI.EU

A Minute-Level High-Frequency Data Acquisition and Lightweight Edge Diagnosis Algorithm for Low-Voltage Distributed Photovoltaic Systems Based on a Temporal Graph Convolutional Network

Xuekai Hu[1], Shiwei Xue[1], Xingzhi Chang[2], Kun Jiang[2, *], Da Zhang[1]

[1] State Grid Hebei Electric Power Research Institute, Shijiazhuang, Hebei 050021, China
[2] Ningxia Longji Ningguang Instrument Co., LTD, Yinchuan, Ningxia 750021, China

Abstract

The performance disparities and operational characteristics among diverse devices within low-voltage distributed photovoltaic (PV) systems lead to variations in fault manifestations. The limited sampling frequency inherent in conventional approaches fails to capture critical fault features and temporal information in a timely manner. Moreover, the presence of periodic fluctuations in PV fault data contributes to persistently high false alarm rates. This paper proposes a high-frequency, minute-level data acquisition framework and a lightweight edge diagnosis algorithm for low-voltage distributed PV systems based on a temporal graph convolutional network. The proposed approach employs intelligent PV edge terminals to enable high-frequency data acquisition from distributed PV generation units. A graphical representation of the low-voltage distributed PV plant is constructed, from which dynamic temporal features of PV generation data are extracted using temporal convolutional layers, while topological correlations among PV devices are captured through graph convolutional layers. This enables the spatiotemporal joint modeling of fault characteristics. To accommodate the computational constraints of edge devices, a customized adaptation of the MobileNet-V3 architecture is introduced. By integrating attention mechanisms and implementing layer pruning, the model is tailored for enhanced performance in photovoltaic fault classification, thereby achieving lightweight edge diagnosis. Experimental results demonstrate that the proposed algorithm accurately diagnoses output voltage fluctuation faults in PV inverters and effectively identifies abnormal phase voltage fluctuation faults. It achieves high precision, recall, and F1 scores across various fault types. The model exhibits rapid training convergence with a low loss function value, satisfying the requirements for lightweight edge diagnosis in low-voltage distributed PV systems.

Keywords: Temporal Graph Convolutional Network; Low-Voltage Distributed Photovoltaics; High-Frequency Data Acquisition; Lightweight Processing; Edge Diagnosis

Received on 20 August 2025, accepted on 01 May 2026, published on 12 August 2026

doi: 10.4108/ew.14123

1. Introduction

Low-voltage distributed photovoltaic (PV) power generation, which can be directly integrated into the end of the distribution grid, offers flexible deployment and enables on-site consumption, thereby reducing long-distance transmission losses [1]. This approach enhances the resilience and local supply capacity of urban energy systems and has emerged as a key direction for energy transformation. The distribution grid is currently experiencing a surge in the integration of low-voltage distributed PV systems, which consequently poses challenges to the reliability and security of power system operations [2]. The system primarily faces failures such as module hot spots and degradation, DC-side arcing, inverter power device failures, and voltage violations induced by grid connection [3]. However, fault diagnosis in this context encounters multiple difficulties. Distributed PV systems typically comprise a large number of geographically dispersed sites, and data monitoring is often incomplete, complicating the early detection or identification of latent

* Corresponding author. Email: jsa_771@163.com

faults [4]. Traditional diagnostic methods rely on centralized cloud computing, which necessitates uploading massive time-series data to servers, resulting in high communication latency and difficulty in meeting minute-level response requirements [5]. Although localized diagnostic solutions can mitigate latency, they are constrained by the memory and computational capacity of edge devices, making it challenging to directly deploy complex deep learning models and limiting diagnostic precision [6].

Numerous studies have proposed various fault diagnosis and protection schemes for low-voltage distributed PV distribution networks. Reference [7] introduces a fault diagnosis method for PV-fed cascaded H-bridge five-level inverters based on a residual network. This method effectively extracts fault features through a residual connection structure, achieving high-precision fault identification and localization. To address the susceptibility of PV inverters to noise interference, a noise signal training strategy is incorporated, significantly enhancing model robustness under complex operating conditions. Although this approach demonstrates high diagnostic precision in both single- and double-switch fault scenarios, it suffers from high communication latency, leading to substantial delays in fault diagnosis. In their multi-stage review framework for PV systems, Reference [8] leverages artificial intelligence to address three core tasks: identifying recurring fault types, quantifying their operational impact, and forecasting imminent critical failures. By accurately identifying fault features and evolution patterns, this framework effectively reduces the risk of system downtime and enhances operational reliability. The predictive model can anticipate PV system faults in advance, lowering maintenance costs and providing an effective solution for intelligent operation and maintenance throughout the PV lifecycle. However, this method struggles to handle the high dimensionality of operational data in distributed PV power stations, and diagnostic precision for faults requires further improvement. Reference [9] proposes a fault detection strategy for PV arrays that integrates model fusion. The strategy employs a multi-channel one-dimensional convolutional neural network to learn multi-scale features from the data, and constructs a stacked ensemble framework by fusing LSTM, AdaBoost, and logistic regression models. Accurate classification of PV array fault types is achieved through multi-model collaborative prediction. This approach effectively enhances the robustness of fault diagnosis in complex environments, but it remains difficult to implement real-time diagnosis at the edge. Reference [10] introduces a PV array fault prediction and diagnosis method based on current-voltage conversion. Fault pre-judgment is achieved by comparing differences between reference I-V curves and measured curves, and fault type identification is completed using the distinct I-V characteristics of typical faults such as short circuits, open circuits, hot spots, and degradation. Further extraction of key features, including curve slope and fill factor, combined with fault label training of classification models, enables quantitative diagnosis of fault severity. This method demonstrates high precision in fault type identification and severity diagnosis under complex operating conditions, yet it lacks sensitivity in detecting subtle anomalies.

This paper proposes a minute-level high-frequency acquisition and lightweight edge diagnosis algorithm for low-voltage distributed PV systems based on a temporal graph convolutional network. The approach achieves minute-level high-frequency data acquisition from low-voltage distributed PV installations through photovoltaic intelligent edge terminals. By employing graph structure modeling, it captures topological relationships among devices and utilizes one-dimensional convolutional kernels to perceive and extract features from time-series data of PV power stations. A multi-level convolutional deep network model is established, integrating temporal convolution to extract evolving temporal characteristics. Model training is subsequently optimized via a modified MobileNet-V3 lightweight architecture. The optimized graph convolutional neural network model is deployed on edge devices to enable minute-level fault diagnosis.

2. Construction of the Temporal Graph Neural Network Model

Voltage, current, power, and other operational data are collected from low-voltage distributed photovoltaic systems via photovoltaic intelligent edge terminals, forming a time-series dataset. A graph-based model of the low-voltage distributed photovoltaic power station is constructed to establish a spatial correlation graph. The time-series data are then integrated with the spatial correlation graph to form a spatiotemporal graph structure, which serves as the input for the temporal graph neural network.

2.1. Minute-Level High-Frequency Acquisition of Low-Voltage Distributed Photovoltaic Data

The Photovoltaic Intelligent Edge Terminal (PVIET) is a novel smart operation and maintenance device for distributed photovoltaic systems, equipped with functions such as data acquisition, processing, storage, and uploading. It lays the foundation for effectively addressing the challenges associated with difficult, costly, and inefficient operation and maintenance of distributed photovoltaic installations, while also providing data resources for fault diagnosis in dispersed photovoltaic systems [11]. Given the relatively high cost of a single PVIET, multiple distributed photovoltaic stations typically share one terminal in practical large-scale applications to reduce overall costs. Ensuring the economic efficiency of PVIET configuration while maintaining the reliability and precision of operation and maintenance data acquisition in complex communication environments is an urgent issue that requires resolution.

The PVIET serves as a critical data support device for the smart operation and maintenance of distributed photovoltaic installations. Its primary functions include: 1 communicating with on-site inverters to acquire measurement data, such as total and string-level DC power from the photovoltaic plant [12]; ② collecting module-level metrics - including voltage, current, and temperature - via monitoring equipment at the generation station, aggregated by on-site data collectors; ③ interfacing with integrated fault recording devices to obtain real-time data and perform subsequent analysis; ④ storing the acquired photovoltaic data in a structured format that incorporates local timestamps, while enabling data upload to the cloud; ⑤ addressing the current limitation of data collectors on the market, which generally lack data analysis and processing capabilities. By preprocessing photovoltaic data locally, the PVIET enhances the responsiveness of downstream analytical tasks and alleviates computational burdens on cloud infrastructure [13]. Furthermore, given the diversity of equipment suppliers for distributed photovoltaic stations - characterized by varied communication methods, inconsistent protocols, and significant differences between intelligent and non-intelligent devices - integrating data and status information from multiple device types presents a considerable challenge. To address this, the PVIET supports multiple communication methods, as illustrated in Figure 1.

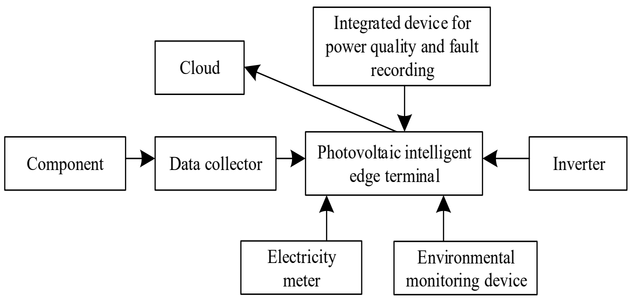

Figure 1. Communication Modes of the PVIET

As the core data acquisition node in low-voltage distributed photovoltaic systems, the PVIET is equipped with robust local computing and communication capabilities. Through its built-in high-precision analog input module, it can directly access real-time signals from photovoltaic inverters, smart meters, and environmental monitoring sensors. The terminal performs synchronous acquisition and processing of electrical parameters - such as voltage, current, and power - along with environmental data - including irradiance and temperature - at the local level. It utilizes a high-performance processor for raw data aggregation and compression at sub-second or even millisecond-level resolution. The key to achieving minute-level high-frequency data acquisition in low-voltage distributed photovoltaic systems lies in the edge computing architecture adopted by the PVIET [14]. Deployed on-site at photovoltaic installations, the terminal rapidly establishes a network with various devices within the station using the Modbus standard protocol. It features multi-task parallel processing capabilities, enabling uninterrupted polling and acquisition of dozens of data points simultaneously. Subsequently, relying on its built-in 4G/5G or fiber-optic communication module, the terminal continuously uploads aggregated data to the cloud or a regional master station at minute-level intervals, thereby achieving high-frequency acquisition of photovoltaic power generation data and providing a real-time data foundation for refined power grid management.

2.2. Graph Modeling of Low-Voltage Distributed Photovoltaic Power Stations

To enable the graph convolutional network to process data from low-voltage distributed photovoltaic systems, graph-based modeling is performed on photovoltaic power stations by analyzing the correlations among the power generation of multiple stations within a region. Figure 2 depicts the actual spatial distribution of photovoltaic power stations, while Figure 3 illustrates the node-edge topological structure derived from the graph modeling process.

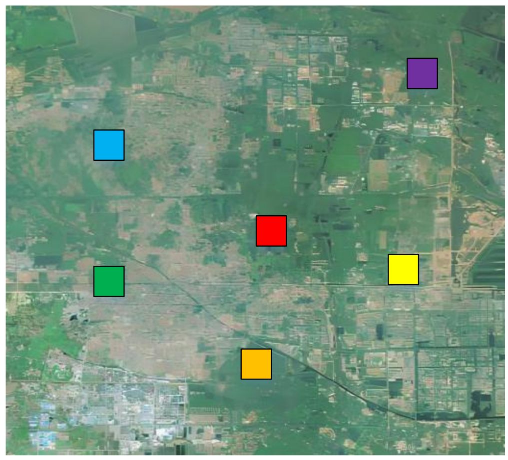

Figure 2. Actual Distribution of Photovoltaic Power Stations

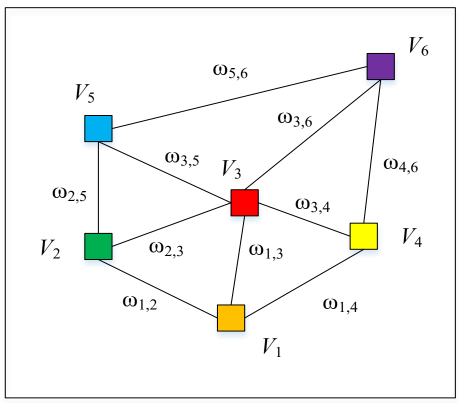

Figure 3. Topological Structure of a Photovoltaic Power Station

Each photovoltaic power station within a given region is represented as a node, and the correlations between nodes are represented by weighted edges. The set of photovoltaic power stations in the region at time t can be represented as a spatiotemporal graph in the following form:

$$\vartheta_t = \langle \kappa_t, \mu \rangle \tag{1}$$

$$\kappa_t = \{ v_{m,t} \} (m = 1, 2 \ldots, n) \tag{2}$$

$$\mu = \{ \omega_{m,j} \} (m, j = 1, 2 \ldots, n) \tag{3}$$

In Equations (1)-(3), $\kappa_t = \{ v_{m,t} \}$ denotes the set of power output records at time t. For all nodes in the spatiotemporal graph, $\mu = \{ \omega_{m,j} \}$ represents a spatiotemporal graph with weighted edges, forming a weighted adjacency matrix. Here, $\omega_{m,j}$ denotes the coupling coefficient between nodes v_m and v_j. An edge is established between nodes v_m and v_j only when a strong correlation exists between them. The weight coefficient between nodes can be expressed as:

$$\omega_{i,j} = \begin{cases} e^{-(v_i, v_j)}, r_{i,j} > k \\ 0, r_{i,j} \le k \end{cases} \tag{4}$$

In Equation (4), $r_{i,j}$ represents the correlation coefficient between two nodes, and (v_i, v_j) denotes the Euclidean distance between two nodes.

If $r_{i,j} > k$, this indicates a strong correlation between the two photovoltaic power stations, and nodes v_i and v_j can be connected by an edge. Conversely, if $r_{i,j} \le k$, no connection is established between the nodes.

3. Lightweight Edge Diagnosis of Photovoltaic Systems Based on Temporal Graph Convolutional Networks

3.1. Minute-Level High-Frequency Acquisition of Low-Voltage Distributed Photovoltaic Data

Low-voltage distributed photovoltaic power stations generate massive amounts of data daily, produced by power generation equipment distributed across different areas and groups. The equipment types within each area and group are consistent, and the types of faults that occur are similar; therefore, fault diagnosis can be performed based on the operating status of each equipment group.

Based on daily maintenance records, the analysis identifies several recurrent fault types, primarily including: photovoltaic panel obstruction faults, inverter operational failures, short-circuit incidents, and voltage anomalies [15]. Photovoltaic panel obstruction faults mainly manifest as hot spots on the panels, typically caused by physical blockage. This issue is generally reflected in the data as a significant decrease in inverter current. Inverter operational failures often result in elevated voltage levels, which can lead to abnormal inverter operation [16]. A short circuit at the inverter output terminal typically induces a rapid increase in circuit current [17]. Voltage anomalies refer to three-phase voltage values exceeding the normal range, generally caused by excessively low or high three-phase impedance. Common fault types and their associated manifestations are summarized in Table 1.

Table 1. Fault Categories of Low-Voltage Distributed Photovoltaic Systems

Fault Type	Causes and manifestations of faults
Photovoltaic panel shading fault	Obstruction coverage leads to a significant decrease in inverter current
Inverter operation failure	The inverter's three-phase imbalance leads to abnormal current or high voltage, resulting in abnormal DC output from the inverter
Inverter short circuit fault	The short circuit at the inverter output terminal causes the circuit current to rapidly increase
Abnormal voltage value fault	The three-phase impedance is either too low or too high, resulting in the phase voltage being too high and exceeding the allowable range

3.2. Construction of the Temporal Graph Convolutional Network Model

3.2.1. Photovoltaic Fault Temporal Feature Extraction Based on a Temporal Convolutional Layer

One-dimensional convolutional operations are employed to extract local patterns from the time series of photovoltaic power generation data, thereby capturing the instantaneous changes induced by faults. Gated linear units (GLUs) are utilized to learn time-based features from power generation time series of varying lengths. A schematic diagram of the temporal feature extraction module is presented in Figure 4.

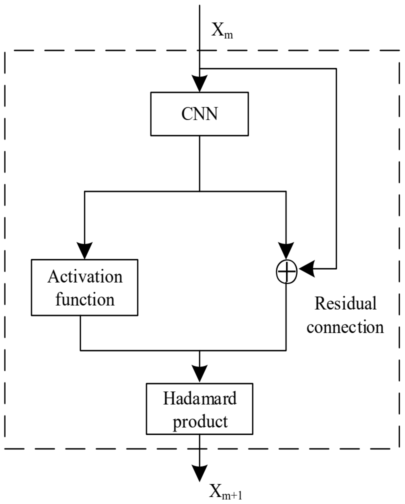

Figure 4. Structure of the Temporal Feature Extraction Module

The input to the gated linear unit is historical power generation data. Let $X_m \in R^{N\times C^i}$, where C^i denotes the number of channels in the input time series and N represents the length of the input time series. A convolutional kernel $\Gamma \in R^{K_t \times C^i \times 2C^0}$ is employed to perform one-dimensional convolution on the input sequence X_m, yielding the following output:

$$X'_m = \Gamma * X_m \in R^{(N-K_t+1)\times 2C^0} \tag{5}$$

In Equation (5), K_t denotes the size of the convolution kernel, and c^0 represents the number of output channels. The input X'_m is split into two identical parts. One part is connected to the input via a residual connection, while the other part is activated using the Sigmoid function [18]. Finally, the convolution outputs of the two parts are combined via the Hadamard product to yield the output of the temporal convolution module: $X_{m+1} \in R^{(N-K_t+1)\times C^0}$.

3.2.2. Spatial Feature Learning of Photovoltaic Faults Using Graph Convolutional Networks

Node-specific spatial attributes within a node-edge topological graph of the photovoltaic power station are extracted using a graph convolutional network [19]. Meanwhile, the normalized Laplacian matrix is employed in the frequency domain to represent the graph topology of the photovoltaic power station as follows:

$$L = I - D^{-\frac{1}{2}} E D^{\frac{1}{2}} \tag{6}$$

In Equation (6), I denotes the identity matrix, and E represents the Laplacian matrix derived from the graph structure of photovoltaic power generation. Let $D = \{d_{i,i}\} \in R^{N\times N}$ be the degree matrix of the graph describing power generation in the photovoltaic plant, where $d_{i,i} = \sum_j \omega_{i,j}$.

By performing eigendecomposition on the normalized Laplacian matrix, we obtain $L = U\Lambda U^T$, with $U \in R^{N\times N}$ being the matrix of eigenvectors and $\Lambda = [\lambda_1, \lambda_2, \ldots, \lambda_n]$ the diagonal matrix of eigenvalues.

The graph convolution equation is then given by:

$$\left(X_m * g\right) = U\left(U^T g\right)\otimes\left(U^T X_m\right) \tag{7}$$

In Equation (7), X_m denotes the input to the graph convolutional network, which corresponds to the output tensor from the temporal convolution module. The parameter g serves as the convolution weight, and $\otimes$ represents the Hadamard product. By adopting $g_\vartheta = U^T g$ as the convolution kernel, the resulting expression for graph convolution is given as follows:

$$\left(X_m * g\right) = U g_\vartheta U^T X_m \tag{8}$$

Owing to the substantial computational load associated with graph convolution, Chebyshev polynomials are employed to approximate the convolution kernel in order to enhance the speed of spatial feature extraction [20]. This yields the following expression for the convolution kernel:

$$g_\vartheta = g_\vartheta\left(\Lambda\right) \approx \sum_{H=0}^{H-1} \theta_H T_\theta\left(\tilde{\Lambda}\right) \tag{9}$$

In Equation (9), $\tilde{\Lambda}$ denotes the scaled eigenvalue matrix of Λ, T_θ represents the coefficient vector of the Chebyshev polynomial, and $T_\theta\left(\tilde{\Lambda}\right)$ is the Chebyshev polynomial itself.

By incorporating the Chebyshev polynomial, the graph convolution equation can be reformulated as follows:

$$g * x = \sum_{H=0}^{H-1} \theta_H T_\theta\left(\tilde{L}\right) x \tag{10}$$

After passing through the temporal feature extraction module, the output $X_{m+1} \in R^{(N-K_t+1)\times Ci}$ of the historical power generation data from the photovoltaic power station is convolved with the weighted adjacency matrix $E = \{\omega_{i,j}\}$ via spatial convolution, yielding the following output: $X_{m+2} \in R^{(N-K_t+1)\times C0}$.

3.3. Construction of the Temporal Graph Convolutional Network Model

Deploying optimized graph convolutional network models on edge devices enables edge-based fault diagnosis without reliance on cloud servers. However, as model depth and complexity increase, this can lead to slower response times and delayed fault identification. By introducing the MobileNet-V3 lightweight architecture and adapting it based on the MobileNet-V3 Large variant, it is possible to simultaneously enhance the classification precision of the graph convolutional network and improve computational speed, thereby achieving minute-level real-time fault diagnosis.

3.3.1. MobileNet-V3 Architecture

The fundamental building block of MobileNet-V3, termed the bottleneck (bneck) and illustrated in Figure 5, integrates three core operations. First, it employs factorized convolutions to reduce computational overhead. Second, it adopts an inverted residual connection with linear bottlenecks to facilitate gradient flow. Third, it incorporates a squeeze-and-excitation module to perform feature recalibration, thereby enhancing the network's representational capacity. Supported by the aforementioned architecture, the MobileNet-V3 model achieves a significant reduction in both computational complexity and parameter count compared to traditional convolutional neural networks, greatly accelerating the speed of fault diagnosis. Furthermore, the model is capable of learning progressively more granular image features, which in turn improves classification precision. NL denotes the type of activation function, which can be selected as HS (H-Swish) or RE (ReLU).

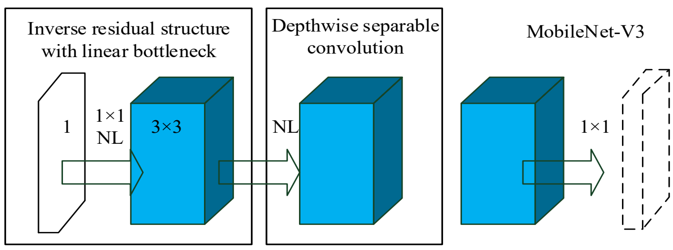

Figure 5. Structure of the Bottleneck (Bneck)

(1) Depthwise Separable Convolution

The core concept underlying the MobileNet series is the replacement of standard convolution with depthwise separable convolution. The computation in depthwise separable convolution is performed in two stages. The process begins with the application of a convolution filter to each input channel independently, a step known as depthwise convolution. Subsequently, pointwise convolution (i.e., 1×1 convolution) is applied to combine the output channels of the depthwise convolution. By adopting this approach, both computational complexity and the number of parameters are reduced, leading to shorter training times and a significant improvement in fault diagnosis speed. However, this reduction in complexity is accompanied by a marginal decrease in diagnostic precision.

Given an input feature map of size (D_F, D_F, M), the convolution kernel is of size: (N, D_K, D_K, M) and the output feature map has dimensions (D_G, D_G, N). The computational complexity and parameter count for conventional convolutional layers are given as follows:

$$P_1 = D_G \cdot D_G \cdot D_K \cdot D_K \cdot N \cdot M \tag{11}$$

$$C_1 = (D_K \cdot D_K \cdot M) N \tag{12}$$

The parameter counts for depthwise separable convolution are given as follows:

$$P_2 = D_G \cdot D_G \cdot D_K \cdot D_K \cdot M + D_G \cdot D_G \cdot M \cdot N \tag{13}$$

$$C_2 = D_K \cdot D_K \cdot M + M \cdot N \tag{14}$$

The ratio of computational complexity and parameter count between the two approaches is expressed as follows:

$$\frac{P_2}{P_1} = \frac{C_2}{C_1} = \frac{1}{N} + \frac{1}{D_K^2} \tag{15}$$

In practical network implementations, the value of N is significantly larger than D_K^2. According to Equation (15), depthwise separable convolution achieves a reduction in both computational cost and parameter count by a factor of D_K^2 compared to traditional convolution, thereby substantially shortening the training time.

(2) Inverted Residual Module with Narrow Linear Layers

Infrared images of photovoltaic module defects typically exhibit low contrast, which necessitates the adoption of a structure capable of learning finer details of such defects to improve classification precision. The linear bottleneck in MobileNet-V3 refers to a convolutional layer whose filters are combined with a linear activation function. This structure enhances model performance by expanding the feature dimensions, employs skip connections to mitigate gradient vanishing, accelerates model training, and enables the extraction of finer image details through deconvolution-based mapping.

(3) Squeeze-and-Excitation (SE) Module

The SE module assigns different weights to each feature map, enabling the model to focus on more informative features.

3.3.2. Improved MobileNet-V3 Network

To further enhance the precision and computational speed of fault classification, and to address the limitations of the MobileNet-V3Large architecture, this paper proposes an improved network based on MobileNet-V3Large by optimizing the activation function and classifier.

(1) Activation Function Optimization

Activation functions are a crucial component in neural networks, as they determine the network's learning capability. The original MobileNet-V3 adopts the H-Swish activation function to handle the extensive and heterogeneous nature of photovoltaic module defect data. However, given the large volume of data and the diversity of fault types present in photovoltaic module defect images, there is a need for an activation function that is more efficient, robust, and simpler than H-Swish. To address this, this paper opts to replace the H-Swish activation function with the TanhExp activation function.

The formulation of TanhExp is given as follows:

$$F(x) = xTanh\left[\exp(x)\right] \tag{16}$$

TanhExp is a continuous function that permits negative values, which helps mitigate the gradient vanishing problem and improve convergence speed. It also accelerates parameter updates within the network, thereby further expediting the learning process. The application of TanhExp can significantly enhance the overall recognition rate of the model, effectively improving both the diagnostic speed and classification precision for multi-class classification tasks.

(2) Classifier Optimization

To further improve classification precision, the L2-SVM classifier is adopted in place of the original classifier in MobileNet-V3. Given the training data $(x_n, t_n), n = 1, 2, ..., N, x_n \in R^D, t_n \in \{-1, 1\}$, the support vector machine (SVM) model is formulated as follows:

$$\begin{cases} \min \frac{1}{2}\psi^T\psi + Y\sum_{i=1}^{N}\xi_n \\ s.t. \psi^T x_n t_n \geq 1 - \xi_n \forall n \\ \xi_n \geq 0 \forall n \end{cases} \tag{17}$$

In Equation (17), ψ denotes the normal vector of the optimal hyperplane, Y is a parameter used to adjust the proportion of misclassified samples, and ξ_n represents the slack variable.

The objective function of L2-SVM is given as follows:

$$\min \frac{1}{2}\psi^T\psi + C\sum_{i=1}^{N}\max\left(1 - \psi^T x_n t_n, 0\right)^2 \tag{18}$$

For the low-voltage distributed photovoltaic test data, the fault diagnosis categories are defined as follows:

$$g(x) = \arg\max\left(\psi^T x\right)t \tag{19}$$

4. Experimental Analysis

In the experiment, a low voltage level of 0.38 kV (based on the IEEE 21-bus system) is selected as an example to simulate a low-voltage distributed photovoltaic distribution network. The corresponding network topology is illustrated in Figure 6.

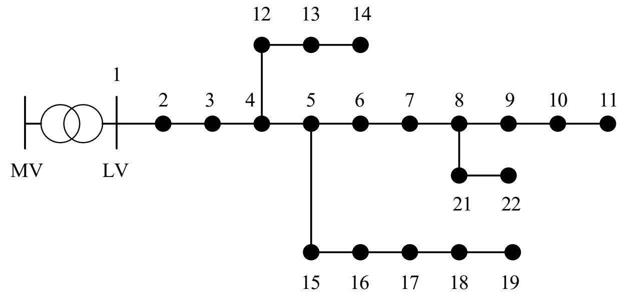

Figure 6. Topological Structure of the Photovoltaic Power Distribution Network

Figure 6 depicts a low-voltage 21-node distribution network, in which nodes 6, 8, 9, 10, 13, 15, 19, 21, and 22 serve as low-voltage access points. The network parameters are presented in Table 2.

Table 2. Parameters of the Low-Voltage Distributed Photovoltaic Power Distribution Network

Parameter	Numerical value
Rated voltage of photovoltaic distribution network / V	380
Power reference value / kW	300
Rated power/kW	100
PV maximum operating current / A	4.62
Maximum working voltage of PV / V	42.8
DC load / W	0~300
Rated power of PV grid-connected converter / W	200
DC bus capacitance value / μF	3300

The experimental data are derived from the operation logs of a photovoltaic power station spanning October 2024 to June 2025. The logs comprise 72 data entries, including power generation, on-grid energy, daily power generation, voltage, and current. A comparative analysis with fault maintenance records reveals that faults frequently occur in photovoltaic modules. Furthermore, when examined in conjunction with operational data recorded during fault events, it is observed that abnormal operational data are often reflected in the inverter under fault conditions.

Based on the aforementioned observations, an abnormal voltage signal is injected using an adjustable DC power supply to simulate inverter output voltage fluctuations. The methods described in References [7] and [8], along with the proposed method, are employed to diagnose the inverter output voltage fluctuation fault. The corresponding voltage waveform is illustrated in Figure 7.

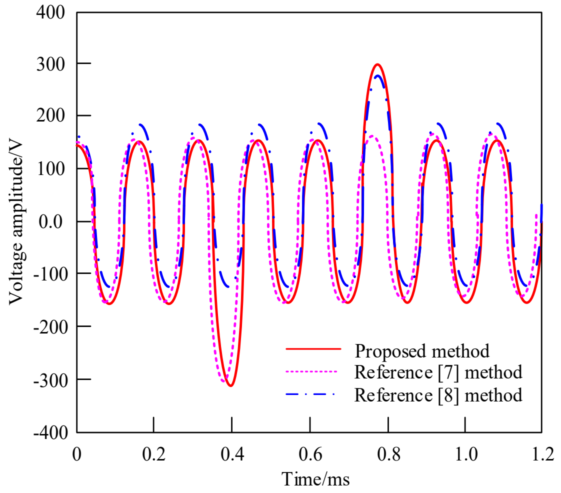

Figure 7. Inverter Output Voltage Waveform

As illustrated in Figure 7, the proposed method accurately identifies abnormal voltage fluctuations at both 0.4 ms and 0.8 ms. In contrast, the method described in Reference [7] identifies voltage fluctuations only at 0.4 ms, while the method in Reference [8] identifies fluctuations solely at 0.8 ms. By leveraging a temporal graph convolutional network that integrates the temporal characteristics of low-voltage distributed photovoltaic distribution networks, the proposed method is capable of accurately extracting feature quantities - representative of inverter faults - from voltage waveforms, thereby enabling precise diagnosis of photovoltaic inverter output voltage fluctuation faults.

When the three-phase impedance of a low-voltage distributed photovoltaic distribution network is excessively high, it can lead to voltage anomalies, causing phase voltages to exceed the permissible range. The methods presented in References [7] and [8], along with the method proposed in this study, are employed to test the phase voltages of the photovoltaic distribution network under high three-phase impedance conditions. The comparative results are presented in Figure 8.

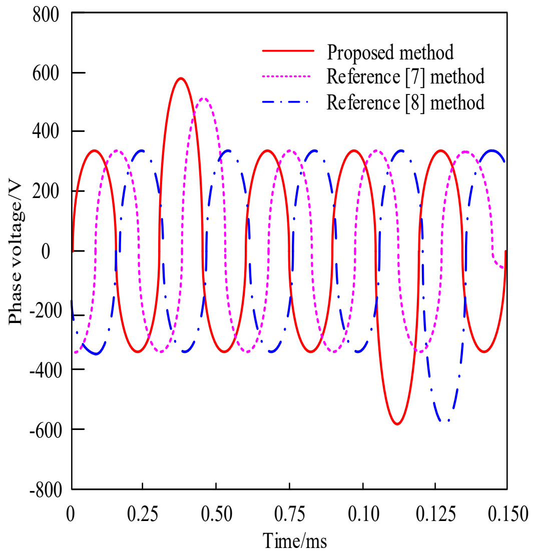

Figure 8. Phase Voltage of the Photovoltaic Distribution Grid

As analyzed in Figure 8, the residual network method presented in Reference [7] is capable of identifying phase voltage high faults, yet it fails to detect phase voltage low faults, primarily due to its reliance on single temporal feature extraction. The multi-stage review framework described in Reference [8] accurately identifies phase voltage low faults; however, it exhibits a significant response delay and demonstrates insufficient capability in capturing transient overvoltages. In contrast, the proposed method, which integrates a graph neural network with an improved MobileNet-V3 model, not only accurately identifies phase voltage high faults but also provides real-time early warning of voltage violations, significantly outperforming the comparative approaches. This validates its real-time performance and robustness in diagnosing voltage anomalies.

Based on the above, the lightweight edge diagnosis performance of the three methods is evaluated. The sample data from the low-voltage distributed photovoltaic distribution network are divided into two subsets: 70% allocated as the training set and 30% as the validation set. Historical sample data from November 2025 are used as the test set. Table 3 presents the precision, recall, and F1-scores achieved by the temporal graph convolutional network for different fault types.

Table 3. Results of the Temporal Graph Convolutional Network on the Test Set

Category	Precision /%	Recall /%	F1-score/%
Normal	98.75	98.97	99.10
Photovoltaic panel shading fault	99.98	99.21	99.83
Inverter operation failure	99.79	99.36	99.64
Inverter short circuit fault	99.65	99.57	99.72
Abnormal voltage value fault	99.32	99.64	99.41

As shown in Table 3, the temporal graph convolutional network demonstrates strong performance across various fault types. The proposed method extracts spatial topological features - such as those associated with photovoltaic arrays and inverters - through the graph convolutional layer. Simultaneously, it captures dynamic temporal features, including minute-level voltage fluctuations, via the temporal convolutional layer, thereby identifying the transient or persistent characteristics of faults. Furthermore, hierarchical temporal convolution is employed to extract both minute-level transient features and hourly-level trend features concurrently, enabling high-frequency, minute-level data acquisition for low-voltage distributed photovoltaic systems. Using the methods from References [7] and [8] as benchmarks, the changes in precision and loss function during the training process of the three models are illustrated in Figure 9.

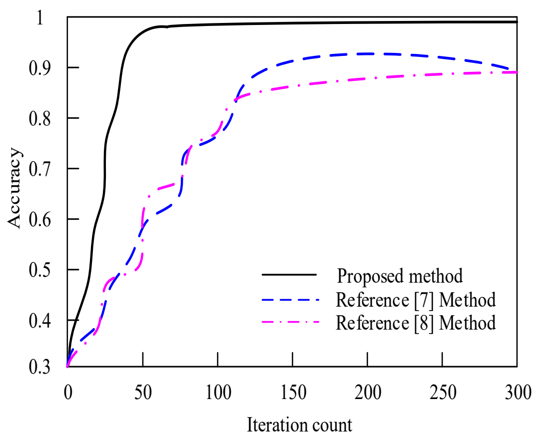

(a) Precision

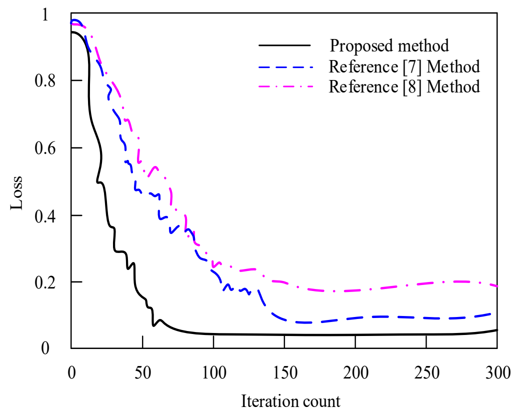

(b) Loss Function

Figure 9. Changes in Precision and Loss Function During Model Training

As can be observed from Figure 9, the precision of the method from Reference [7] tends to converge stably after approximately 150 training iterations, while the method from Reference [8] achieves stable convergence after around 100 iterations. In contrast, the proposed method converges stably after only 50 training iterations. During the training process, the precision value increases continuously, with the proposed method attaining the highest precision of 0.99. Simultaneously, the loss value decreases progressively, with the proposed method achieving the lowest loss of 0.04. The proposed method incorporates an improved MobileNet-V3 model and selects the TanhExp activation function to mitigate the vanishing gradient problem, thereby accelerating convergence. Furthermore, it employs L2-SVM as a classifier to enhance training precision. These results demonstrate that deploying the improved MobileNet-V3 model directly on low-voltage distributed photovoltaic edge devices enables lightweight edge diagnosis for such systems, thereby satisfying real-time diagnostic requirements.

5. Conclusion

The minute-level high-frequency acquisition and lightweight edge diagnosis algorithm for low-voltage distributed photovoltaic systems proposed in this paper, which is based on a temporal graph convolutional network, employs photovoltaic intelligent edge terminals to achieve minute-level high-frequency data acquisition from distributed photovoltaic generation units. By integrating a graph convolutional network with gated linear units, the algorithm accurately extracts the spatiotemporal characteristics of fault data. Leveraging the advantages of the improved MobileNet-V3 architecture - namely, fast fault diagnosis speed and high classification precision - it effectively resolves the trade-off between real-time performance and diagnostic precision for minute-level high-frequency data in low-voltage distributed photovoltaic systems. Experimental validation demonstrates that the proposed method achieves high precision in diagnosing photovoltaic inverter output voltage fluctuation faults and phase voltage anomalies. Furthermore, the algorithm exhibits superior training speed and diagnostic precision compared to the benchmark methods. This algorithm can be widely applied in the detection, operation, and maintenance of distributed photovoltaic power stations, offering a novel solution for power inspection and fault analysis.

Acknowledgements
The study was supported by “State Grid Hebei Electric Power Co., Ltd. 2025 Science and Technology Project 'Key Technology Research on Smart Perception and Abnormal Diagnosis of Low-Voltage Distributed Photovoltaics - Technology R&D' (kj202508-004)”

References

[1] Han Jie, Jiang Tong, Liang Hao, et al. Stability Control Strategy for Photovoltaic Grid Connected Systems Considering Weak Grid Impedance[J].Computer Simulation,2025,42(3):117-122.
[2] Wu L , Zhang W , Chen W ,et al.A Multi-Time scale optimal scheduling strategy for integrated energy systems considering the power randomness of wind and photovoltaic[J].Electrical Engineering, 2025, 107(7):9109-9123.
[3] Xu H , Yu C , Chen C ,et al.Impedance Model-based Stability Analysis of Single-stage Grid-connected Inverters Considering PV Panel Characteristics and DC-side Voltage[J].Protection and Control of Modern Power Systems, 2025, 10(4):130-145.
[4] Hanrieder N , Kujawa A , Seychelles A B ,et al.Estimation of maximum photovoltaic cover ratios in greenhouses based on global irradiance data[J].Applied Energy, 2024, 365(7):1-9.
[5] Gupta A K , Singh R K .A review of the state of the art in solar photovoltaic output power forecasting using data-driven models[J].Electrical Engineering, 2025, 107(4):4727-4770.
[6] Chakar J , J.-P. C , Bonnassieux Y ,et al.A Bayesian inference approach to extract circuit model parameters and analyze photovoltaic degradation from power production data[J].Solar Energy, 2024, 274(5):1-9.
[7] Ashfaq I , Uddin Z , Islam N U ,et al.Fault diagnosis and localization in photovoltaic-fed cascaded half-bridge five-level inverter using residual network architecture[J].Electrical Engineering, 2025, 107(10):12861-12884.
[8] Hamza A , Ali Z , Dudley S ,et al.A multi-stage review framework for AI-driven predictive maintenance and fault diagnosis in photovoltaic systems[J].Applied Energy, 2025, 393(9):1-38.
[9] Guo F , Fu W , Wang Y ,et al.Research on fault diagnosis method for photovoltaic array based on model fusion[J].Electrical Engineering, 2025, 107(6):8189-8199.
[10] Chen X , Jiang M , Ding K ,et al.Fault Prediagnosis, Type Identification, and Degree Diagnosis Method of the Photovoltaic Array Based on the Current–Voltage Conversion[J].IEEE Transactions on Power Electronics, 2024, 39(12):16708-16719.
[11] Souhe F G Y , Mbey C F , Kakeu V J F ,et al.Optimized forecasting of photovoltaic power generation using hybrid deep learning model based on GRU and SVM[J].Electrical Engineering, 2024, 106(6):7879-7898.
[12] Yue H , Ali M M , Lin Y ,et al.Ultra-Short-Term Forecasting of Large Distributed Solar PV Fleets Using Sparse Smart Inverter Data[J].IEEE transactions on sustainable energy, 2024,15(3):1968-1980.
[13] Fan Y , Wu H , Lin J ,et al.A distributed photovoltaic short-term power forecasting model based on lightweight AI for edge computing in low-voltage distribution network[J].Renewable Power Generation, IET, 2024, 18(16)3955-3966.
[14] Ye J , Liu Y , Yang L ,et al.A Lightweight Edge Computing Neural Network for Online Photovoltaic Defect Inspection[J].IEEE Transactions on Instrumentation and Measurement, 2025, 74(1):1-14.
[15] Bhowmick S , Mukherjee D , Basu T S ,et al.A Three-Phase Four-Leg Neutral Point Clamped Photovoltaic Inverter With Decoupled Active & Reactive Power Control and DC Link Voltage Ripple Minimization Under Unbalanced Grid Operation[J].IEEE Transactions on Power Electronics, 2025, 40(6):1-14.
[16] Debanjan M , Sourav M .Efficient operation of photovoltaic-interfaced reduced switch 11-level inverter using adaptive swarm-based metaheuristic[J].Electrical engineering, 2024, 106(1):521-551.
[17] Khazaeefar S , Valizadeh M , Sarvenoee A K .An improved Z-source multi-level inverter scheme for grid-connected photovoltaic systems[J].Electrical Engineering, 2025, 107(6):8045-8058.
[18] Du X , Huang Q , Yan Z ,et al.Underwater SLAM front-end matching method based on graph convolutional neural network[J].Ocean Engineering, 2025, 331(1):1-13
[19] Li J , Ren X , Zhang F ,et al.Multi-timescale photovoltaic station power prediction based on Reformer model[J].Energy, 2025, 327(7):1-15.
[20] Zhang Y , Hao Q , Zheng W ,et al.User similarity-based graph convolutional neural network for shilling attack detection[J].Applied Intelligence, 2025, 55(5):1-14.